Strong exciton regulation of Raman scattering in monolayer MoS$_2$

Yuanxi Wang[*]

Department of Physics, 2-Dimensional Crystal Consortium, and Material Research Institute, Pennsylvania State University,
University Park, Pennsylvania 16802, USA

Bruno R. Carvalho

Departamento de Física, Universidade Federal do Rio Grande do Norte, Natal, Rio Grande do Norte 59078-970, Brazil

Vincent H. Crespi[†]

Department of Physics, Department of Materials Science and Engineering, Department of Chemistry,
and 2-Dimensional Crystal Consortium, Pennsylvania State University, University Park, Pennsylvania 16802, USA

The weakly screened electron-hole interactions in an atomically thin semiconductor not only downshift its excitation spectrum from a quasiparticle one, but also redistribute excitation energies and wave-function characters with profound effects on the diverse modes of the material response, including the exciton-phonon scattering processes accessible to resonant Raman measurements. Here, we develop a first-principles framework to calculate frequency-dependent resonant Raman intensities that includes excitonic effects and goes beyond the Placzek approximation. We show how excitonic effects in MoS$_2$ strongly regulate Raman scattering amplitudes and thereby explain the puzzling near absence of a resonant Raman response around the *A* and *B* excitons (band-edge excitations which produce very strong signals in optical absorption), and also the pronounced strength of the resonant Raman response from the *C* exciton (a higher-energy excitation arising from parallel valence and conduction bands). Furthermore, this efficient perturbative approach reduces the number of *GW* plus Bethe-Salpeter-equation calculations from two per Raman mode (in finite displacement) to one for all modes and affords a natural extension to higher-order resonant Raman processes.

Low-energy excitations of two-dimensional semiconductors are dominated by very strong excitonic effects, as exemplified by the *A* and *B* excitons arising from band-edge excitations in monolayer MoS$_2$ and the *C* exciton arising from near-parallel valence and conduction bands [1,2]. While excitonic resonances are evident from absorption spectroscopy [3], resonant Raman spectroscopy offers a more multifaceted perspective: The Raman intensity of a phonon mode plotted against laser energies (Raman excitation profile) not only reveals excitonic resonances with resolutions on par with absorption, but also reflects exciton-phonon coupling strengths [4,5]. Raman features emerging upon reaching resonance furthermore capture finite-momentum processes such as higher-order Raman scattering and defect scattering [6–10], both key processes in valleytronics [5,11,12]. The appeal of these rich outputs, combined with the procedural simplicity of Raman measurements (perhaps best attested by Raman's original discovery using sunlight, distilled liquids, and a human eye [13]) contribute to its wide usage. Spectral features in Raman excitation profiles are generally aligned in energy with absorption features for molecules [14–16] and three-dimensional bulk solids [17], with intensities of similar orders of magnitude,

as modulated by electron-phonon interactions. This expectation is confounded by the puzzling near absence of Raman intensity measured at the *A*/*B* exciton energies and the disproportionately higher Raman intensity measured at the *C* exciton in MoS$_2$ [6,18]. This anomaly in two-dimensional (2D) semiconductors suggests an unidentified regulating effect by excitons.

Despite the rich experimental data on Raman measurements of 2D solids, the role of excitons on Raman spectra is rarely modeled at a first-principles level beyond calculating shifted resonance energies, because of the high computational cost of many-body perturbation theory calculations and the sparsity of implementations that consolidate electron-phonon and many-body phenomena. One recent important theoretical advance [19] (implemented in Refs. [20,21]) used finite differences through the solution of the Bethe-Salpeter equation (BSE) on the quasiparticle (*GW*) band structure, but employed a quasistatic Placzek approximation that is only valid in the nonresonant regime. Here, we follow the generalized approach of Ref. [22], valid for solids in the resonant regime, to develop a perturbation framework that goes beyond the Placzek approximation and includes electron-hole interactions. Both ingredients are crucial to capturing exciton-regulated Raman scattering in MoS$_2$, including dramatic differences in the strength of the resonant response in the vicinity of the *A*/*B* and *C* excitons that agree with experiments. We show that band-extrema electron-hole pairs

---
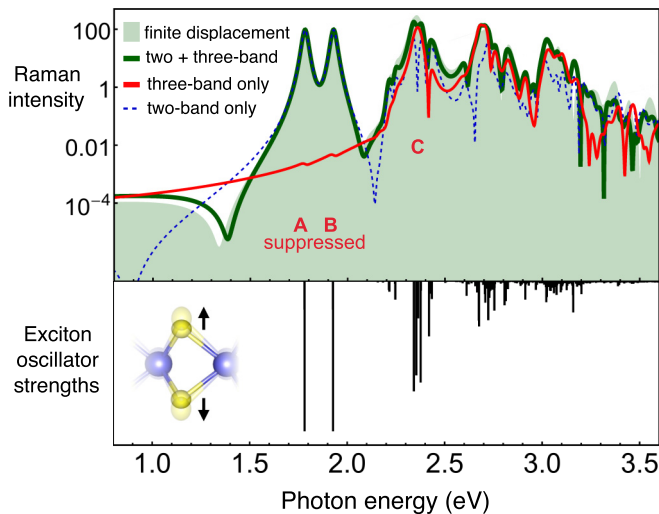
[*]yow5110@psu.edu

[†]vhc2@psu.edu

FIG. 1. Resonant Raman intensities of the out-of-plane A_1' mode in MoS_2 calculated as a function of the laser energy. Combining two-band $|d_2|^2$ (blue dashed) and three-band $|d_3|^2$ terms (red solid) calculated from perturbation theory into $|d_2 + d_3|^2$ (green solid) correctly matches the result from finite displacements (filled light green). Only the three-band plot is to be compared with experiments: Raman intensity is suppressed at the A/B excitons compared with the C exciton. The lower panel shows A/B exciton eigenvalues far below all others and eigenvalues near the C exciton bunched together.

such as the A/B excitons suppress the Raman response due to their energies being well separated from the rest of the exciton spectrum, and that parallel-band electron-hole pairs such as the C exciton amplify the Raman response due to their bunching of energies causing strong rehybridization during atomic vibration.

We first explain the detailed theoretical and computational basis of the calculations; readers interested primarily in the results and physical interpretation of excitonic effects in resonant Raman spectra may advance to Fig. 1 and the associated discussion. First-principles Raman spectra calculations are most straightforward for Raman shifts, routinely achieving excellent agreement with experiments [23–25]. Raman *intensities* are usually computed within the nonresonant Placzek approximation: Since the scattered light intensity is proportional to the electronic susceptibility $\chi(\omega)$ periodically modified by atomic vibrations (ω is the incident light frequency), a product-to-sum identity converts the scattered $\cos(\omega_{phonon}t)\cos(\omega t)$ wave into Stokes and anti-Stokes components [26]. The scattering amplitude depends on how strongly χ is changed by vibrations R, i.e., $|d\chi/dR|^2 \propto |d\epsilon/dR|^2$, where $\epsilon(\omega)$ is the dielectric function $\epsilon(\omega) = 1 + \sum_S |\langle 0|\mathbf{r}|S\rangle|^2/(\omega_S - \omega - i\gamma)$, γ is the lifetime broadening of the excitons, ω_S is the energy of state $|S\rangle$, and S runs over all excitations (the "negative frequency" contribution is suppressed for clarity but is included in all calculations). This derivative has been calculated using the second derivative of the electronic density matrix [27,28], the "$2n + 1$" theorem [29], or finite differences of the static dielectric tensor [24,30] (calculated from density functional perturbation theory [31]). The derivative can also be expanded by treating ω_S and the

matrix elements separately,

$$\frac{d\epsilon(\omega)}{dR} = \sum_S \left(\frac{\partial\epsilon(\omega)}{\partial\omega_S}\frac{d\omega_S}{dR} + \frac{1}{\omega_S - \omega - i\gamma}\frac{d|\langle 0|\mathbf{r}|S\rangle|^2}{dR} \right)$$
$$\equiv d_2 + d_3. \tag{1}$$

Using first-order perturbation theory [32], the former group of "two-band terms"

$$d_2 = -\sum_S \frac{\langle 0|\mathbf{r}|S\rangle\langle S|\partial_R H|S\rangle\langle S|\mathbf{r}|0\rangle}{(\omega_S - \omega - i\gamma)^2} \tag{2}$$

involves only transitions between pairs of bands. The latter group of "three-band terms" (see Supplemental Material [33])

$$d_3 = \sum_{S'\neq S} \frac{-1}{\omega_S - \omega - i\gamma}\left(\frac{\langle 0|\mathbf{r}|S'\rangle\langle S'|\partial_R H|S\rangle\langle S|\mathbf{r}|0\rangle}{\omega_{S'} - \omega_S} \right)$$
$$+ \sum_{S\neq S'} \frac{1}{\omega_{S'} - \omega - i\gamma}\left(\frac{\langle 0|\mathbf{r}|S'\rangle\langle S'|\partial_R H|S\rangle\langle S|\mathbf{r}|0\rangle}{\omega_{S'} - \omega_S} \right)$$
$$= \sum_{S\neq S'} -\frac{\langle 0|\mathbf{r}|S'\rangle\langle S'|\partial_R H|S\rangle\langle S|\mathbf{r}|0\rangle}{(\omega_{S'} - \omega - i\gamma)(\omega_S - \omega - i\gamma)} \tag{3}$$

contains transitions between three states. No phonon-momentum dependence appears since we only focus on the first-order Raman. So far the expressions are general: If all quantities are calculated at the density functional theory (DFT) level, the Hamiltonian $H = H^{DFT}$ [34] and $|S\rangle$ are free electron-hole transitions separated by ω_S; if calculated at the BSE level, $H = H^{BSE}$ [35] and $|S\rangle$ are excitonic wave functions with eigenvalues ω_S. Physically, two- and three-band terms respectively represent contributions from the oscillating excitation *eigenvalues* (Kohn-Sham eigenvalues or BSE eigenvalues) and the oscillatory *rehybridization* of wave functions (Kohn-Sham orbitals or BSE eigenvectors) [36]. By combining the d_2 and d_3 terms we recover the usual perturbation expression for Raman susceptibility α, ignoring small phonon energies,

$$\alpha_{perturb.} \propto \sum_{S,S'} \frac{\langle 0|\mathbf{r}|S'\rangle\langle S'|\partial_R H|S\rangle\langle S|\mathbf{r}|0\rangle}{(\omega_{S'} - \omega - i\gamma)(\omega_S - \omega - i\gamma)}. \tag{4}$$

Phonon frequencies appear explicitly in the more rigorous many-body formulation, where resonant terms becomes equivalent to Eq. (4) in the limit that the phonon frequencies are zero [26,37]. Three-band terms are often neglected due to the apparent squared denominator of the two-band terms [see Eqs. (1) and (2)] [20]; the final expanded expression shows that three-band terms become important when the intervals between excitation energies are small.

So long as laser energies ω are away from excitation levels so that $\omega_{phonon} \ll |\omega - \omega_S + i\gamma|$, the Placzek approximation holds [22] and finite-displacement calculations using static dielectric tensors [24,38] agree qualitatively with Raman intensities measured at finite (but sub-band-gap) ω, due to the near-constant dielectric function in this regime. The use of the Placzek approximation in the resonant regime [19,39] was argued to be problematic in Ref. [22], where a more rigorous expression is derived that is equivalent to keeping only the

three-band terms d_3. These d_3 terms correspond to the so-called "Albrecht B/C terms" (or Herzberg-Teller terms) in the vibronic theory for resonant Raman intensities in molecules accounting for nuclear wave functions [40–42]. The seemingly missing "Albrecht A terms" (or Condon terms) [42] only arise for excitations with finite Frank-Condon shifts and are negligible for delocalized vibrations in solids [43,44] (and even for localized vibrations near certain common defects in MoS_2 [45]).

Since d_3 readily separates from d_2 in the perturbation approach, we derive the single-particle expansion for both at the BSE level and numerically verify that their sum matches the spectra obtained from finite displacements within the Placzek approximation and that, for $\omega \to 0$, d_3 (general) and $d_2 + d_3$ (Placzek) converge to the same value, i.e., d_2 goes to zero. With the optical matrix elements in Eq. (4) readily available in existing GW-BSE codes within the the dipole approximation, we focus on evaluating the exciton-phonon coupling matrix elements $\langle S'|\partial_R H|S\rangle$. For the derivative of the exciton Hamiltonian $\partial_R H^{BSE}$ within the Tamm-Dancoff approximation, we neglect the contribution from the derivative of the BSE kernel ∂K [46], neglect the derivative of the quasiparticle correction by using $\partial_R H^{QP} \approx \partial_R H^{DFT}$ (as validated in Refs. [46,47]) so that

$$d_2 = \sum_{S,vck} \frac{|\langle 0|\mathbf{r}|S\rangle|^2 |S_{vck}|^2}{(\omega_S - \omega - i\gamma)^2}$$
$$\times [\langle ck|\partial_R H^{DFT}|ck\rangle - \langle vk|\partial_R H^{DFT}|vk\rangle], \quad (5)$$

where $S_{vck} = \langle S|vck\rangle$. Here, we neglect $c \neq c'$ and $v \neq v'$ terms in Ref. [46] (DFT-level "three-band" terms) since they only contribute significantly when the energy separation between bands is similar to phonon energies; for the low-energy electronic structure of MoS_2, most band pairs of small separation are up-down-spin copies forbidding interband scattering, with the exception of the valence band top being split by a spin-orbit interaction. Although in general bands split by spin-orbit coupling allow interband scattering (yielding significant DFT-level "three-band" terms [36,48]), the spin-orbit Hamiltonian near the valleys in MoS_2 only involves σ_z so that spins components are decoupled [1,49]. This approximation is numerically justified later. The d_3 terms involve

$$\langle S'|\partial_R H^{BSE}|S\rangle \approx \sum_{vv'cc'k} \langle S'|vck\rangle\langle v'c'k|S\rangle [\langle ck|\partial_R H^{DFT}|c'k\rangle\delta_{vv'}$$
$$- \langle v'k|\partial_R H^{DFT}|vk\rangle\delta_{cc'}]. \quad (6)$$

Again neglecting $c \neq c'$ and $v \neq v'$ terms and substituting into Eq. (3) gives

$$d_3 = \sum_{S \neq S',vck} \frac{\langle 0|\mathbf{r}|S'\rangle\langle S|\mathbf{r}|0\rangle S_{vck} S'^*_{vck}}{(\omega_S - \omega - i\gamma)(\omega_{S'} - \omega - i\gamma)}$$
$$\times [\langle ck|\partial_R H^{DFT}|ck\rangle - \langle vk|\partial_R H^{DFT}|vk\rangle]. \quad (7)$$

All calculations will follow Eqs. (5) and (7).

All GW-BSE calculations are performed using the BERKELEYGW package [50,51] based on Kohn-Sham eigenvalues and orbitals obtained within the local density approximation, using QUANTUM ESPRESSO [52]. An energy cutoff of 24 Ry,

500 empty bands, and a $12 \times 12 \times 1$ k-point grid was used for the dielectric matrix and quasiparticle self-energy, where the Coulomb interaction is truncated in the out-of-plane direction [53]. The static remainder technique [54] accelerates convergence of the quasiparticle gap. BSE matrix elements are assembled using three valence bands and four conduction bands on the same grid and interpolated onto a $40 \times 40 \times 1$ grid for diagonalization (Haydock iteration is not used because BSE eigenvectors are needed). The Supplemental Material [33] contains details on convergence tests for the above parameters and all calculations involving phonons. Finally, summations over the $S \neq S'$ terms are limited to eigenvalue pairs no further apart than 0.3 eV; exciton pairs separated further contribute negligibly due to large denominators in Eq. (7) and their constituent single-particle transitions being from different bands. Increasing this convergence parameter to 0.4 eV changes Raman intensities by at most 2% (for any laser frequency). We include 800 excitonic states to converge Raman intensities within the 0–3.5 eV spectral range.

The calculated Raman intensities $|\alpha(\omega)|^2$ for the out-of-plane A'_1 mode in Fig. 1 show that combining $|d_2|^2$ (blue dashed) and $|d_3|^2$ terms (red solid) from the perturbation approach into $|d_2 + d_3|^2$ (green solid) yields a good agreement with the finite displacement spectrum (filled light green) from preresonance (<1.5 eV) well into the resonant regime, and that two-band terms correctly converge to zero for vanishing laser energies. These agreements are absolute, i.e., with no adjustable rescaling parameter. While the exclusion of $c \neq c'$ and $v \neq v'$ terms (DFT-level three-band terms) proved valid, $S \neq S'$ terms (BSE-level three-band terms) contribute significantly near the C exciton energy ~2.4 eV. Optical transitions within the near-parallel valence and conduction bands along Γ-K (see the band structure in the Supplemental Material [33]) yield a peak in the joint density of states and hence also in the absorbance spectra, ignoring excitonic effects, near 4 eV (blue open in the inset of Fig. 2). Including excitonic effects, these transitions are constituents of the
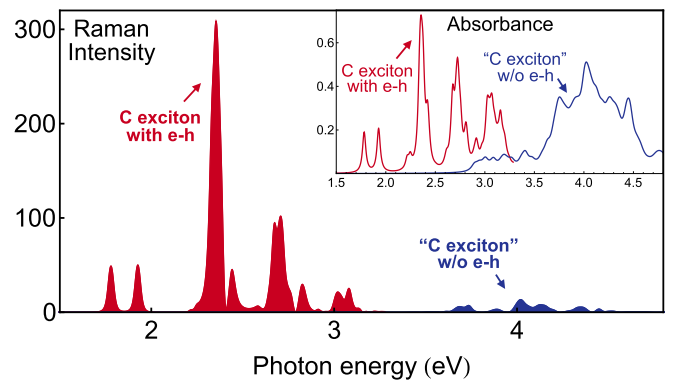

FIG. 2. Raman intensities with (red) and without (blue) excitonic effects, showing the amplified Raman response at the C exciton compared with the Raman intensities calculated without excitonic effects. The inset compares the absorbance spectra with (red, truncated within its range of convergence) and without (blue) electron-hole interaction, where excitonic effects *redistribute* spectral weights without enhancement. Both Raman intensities shown are from finite displacements; the visible A/B resonances here should be suppressed in the more rigorous three-band spectra ($|d_3|^2$ in Fig. 1).

C excitons with BSE eigenvalues bunched near 2.4 eV [1] (red open in the inset of Fig. 2, truncated within its range of convergence). This bunching does *not* cause an order-of-magnitude change in the absorbance spectral features (whose integral is constrained by the f-sum rule [55]), apart from an overall redshift due to the exciton binding energy and a redistribution of spectral weight rendering exciton resonances sharper than single-particle features. However, as in standard perturbation theory where smaller eigenvalue intervals lead to wave functions being more strongly perturbed, bunched BSE eigenvalues cause *strong rehybridization of excitonic states during atomic vibration* [i.e., decreased denominators $\omega_{S'} - \omega_S$ in the first line of Eq. (3)] and regroups what used to be independent transitions at different k points (which cannot scatter into each other by a Γ phonon) into excitonic states all with zero momenta [which allows interscattering, i.e., increased numerator in Eq. (7)]. Therefore, three-band terms contribute an order-of-magnitude amplification in Raman intensities around the C exciton resonance. This can be seen even in the results from finite displacements in Fig. 2, where Raman intensities without an electron-hole interaction near 4 eV (blue filled) are amplified to form the highest Raman peak with an electron-hole interaction near 2.4 eV (red filled); comparing the more rigorous three-band spectra would yield the same conclusion. In stark contrast, the A and B excitons—each doubly degenerate (two valleys)—are well separated from other excitations, so they only contribute to two-band terms (dashed blue in Fig. 1). Since only three-band terms are valid for on-resonance frequencies, the orphaned A and B states should not appear in an experimental measurement. Thus the final frequency-dependent Raman intensity $|d_3|^2$ (red in Fig. 1) is suppressed at the A/B excitons and amplified at the C exciton. In this way, our perturbation method reveals how spectral features in resonant Raman characterize not only the exciton spectrum and wave-function character, but also how exciton-phonon coupling enables interstate scattering.

We now compare with experiments in Fig. 3 and demonstrate that agreement is only achieved for the beyond-Placzek
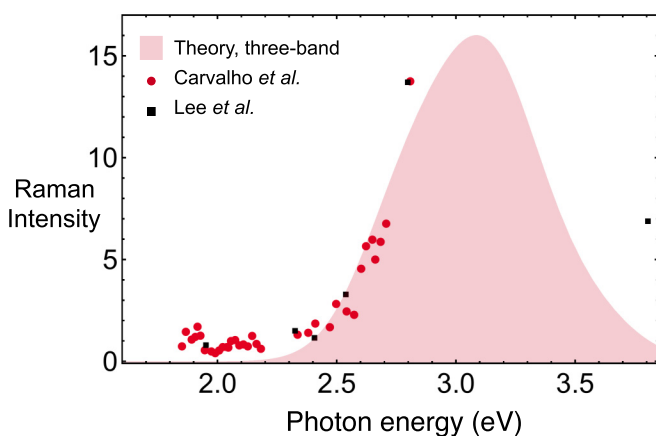
treatment of Raman intensity including excitonic effects. Two sets of experimental data on the frequency-dependent A_1' mode intensity from Refs. [6,18] are aligned at the 2.8-eV data point and normalized in intensity by the Raman peak of silicon at $520\ \text{cm}^{-1}$ (which has its own known frequency dependence) to yield the modulus squared of the Raman susceptibility $|\alpha(\omega)|^2$ (to be distinguished from the Raman cross section, which has an additional ω^4 frequency dependence [36,48]), which can be directly compared with the calculated results. The calculated three-band intensity from Fig. 1 is broadened by 0.2 eV to reflect more realistic C exciton lifetimes estimated from those of free carriers in MoS_2 [56]. Good agreement is achieved for the Raman intensity suppression around the A and B excitons, as clearly resolved by the red points (not missing potential resonances) and for the Raman intensity amplification near the C exciton. The two very small resonances measured at the A/B exciton energies and a scissors shift applied are discussed in the Supplemental Material [33]. In all prior comparisons between finite displacement BSE calculations (Placzek) and experiments known to us, satisfactory agreements were achieved for few laser frequencies [21] or for a limited spectral region (e.g., the lowest excitonic peak in Ref. [19], WS_2 A/B excitons in Ref. [20], and the WSe_2 C exciton in Ref. [20]). Going beyond Placzek allows us to achieve agreement over the energy range of all three excitons.

This analysis has broader implications. For the band structure of a generic solid, every exciton bound state from the solution of the BSE consists of electron-hole pairs with matching group velocities, either at band extrema (zero velocity, spanning a direct gap) or along parallel bands (finite velocity, more common in indirect band-gap materials). We expect band-extrema excitons in general to suppress the Raman response: By construction these excitons have energies well below parallel-band excitons, giving large denominators in Eq. (7). Even when there are multiple degenerate valleys as in the case of MoS_2, the localized (in k-space) nature of band-extrema excitons allows us to approximate the electron-phonon coupling matrix elements to be constants in Eq. (7), so (focusing on one vc pair) the sum $\sum_k \langle S'|k\rangle\langle k|S\rangle$ can be contracted to zero due to the orthogonality of S and S', giving a vanishing numerator. By contrast, we expect parallel-band excitons in general to amplify the Raman response: By construction, parallel pairs of conduction and valence bands span larger Brillouin zone areas (often emanating from high-symmetry points, which gives them a further multiplicative degeneracy factor) and therefore allow abundant ways of assembling into excitons with similar energies bunching in a narrow energy window (as many as there are sampled k points in the parallel-band areas). The resonant Raman intensity of silicon amplified by excitonic effects (compared with the independent quasiparticle case) in Ref. [19] is presumably attributed to this mechanism, given the abundance of parallel bands in silicon [57]. As a consequence of the general validity of the three-band dominance demonstrated here, resonant Raman measurements can directly probe how excitons undergo *interstate* scattering by phonons, which affects exciton population dynamics and lifetimes [58].

The perturbation framework developed here not only allows us to go beyond the classical Placzek approximation

FIG. 3. Experimental Raman excitation profile for the out-of-plane A_1' mode from Ref. [18] (red) and Ref. [6] (black), compared with the calculated three-band terms in Fig. 1 with broadening increased to 0.2 eV to reflect more realistic exciton lifetimes as estimated from free-electron lifetimes.

and include excitonic effects, but also to achieve better scaling behavior: The GW-BSE routine is only performed once statically (at the slight expense of calculating electron-phonon coupling matrix elements for all Raman active modes), compared with finite difference methods where at least two GW-BSE runs are needed for each Raman active mode. This advantage can be exploited to accelerate Raman intensity calculations for low-symmetry materials such as ReS_2 [59], with 18 Raman modes. For second-order Raman intensities, the computational demand for finite differences is even higher, requiring evaluating the BSE dielectric function N^2 times, with N being the number of Raman modes. In addition, finite-momentum phonon displacements need to be performed on supercells compatible with phonon wave vectors. Despite the computational challenge, second-order Raman intensities were successfully calculated from first principles recently [60]. Our perturbation treatment can be naturally extended to calculate the second-order Raman, where the electron-phonon coupling matrix elements would also be calculated for finite-momenta phonons, but without employing supercells owing to density functional perturbation theory. The key challenge would be in efficiently calculating finite-momentum excitons [61,62] (exciton dispersions), which may be overcome using accurate tight-binding-based models (fitted to GW band structures) [63].

[1] D. Y. Qiu, F. H. da Jornada, and S. G. Louie, Phys. Rev. Lett. **111**, 216805 (2013); Phys. Rev. B **93**, 235435 (2016).

[2] R. Soklaski, Y. Liang, and L. Yang, Appl. Phys. Lett. **104**, 193110 (2014).

[3] K. F. Mak, C. Lee, J. Hone, J. Shan, and T. F. Heinz, Phys. Rev. Lett. **105**, 136805 (2010).

[4] B. R. Carvalho, L. M. Malard, J. M. Alves, C. Fantini, and M. A. Pimenta, Phys. Rev. Lett. **114**, 136403 (2015).

[5] B. R. Carvalho, Y. Wang, S. Mignuzzi, D. Roy, M. Terrones, C. Fantini, V. H. Crespi, L. M. Malard, and M. A. Pimenta, Nat. Commun. **8**, 14670 (2017).

[6] J.-U. Lee, J. Park, Y.-W. Son, and H. Cheong, Nanoscale **7**, 3229 (2015).

[7] K. Gołasa, M. Grzeszczyk, P. Leszczyński, C. Faugeras, A. A. L. Nicolet, A. Wysmołek, M. Potemski, and A. Babiński, Appl. Phys. Lett. **104**, 092106 (2014).

[8] S. Mignuzzi, A. J. Pollard, N. Bonini, B. Brennan, I. S. Gilmore, M. A. Pimenta, D. Richards, and D. Roy, Phys. Rev. B **91**, 195411 (2015).

[9] A. C. Ferrari, J. C. Meyer, V. Scardaci, C. Casiraghi, M. Lazzeri, F. Mauri, S. Piscanec, D. Jiang, K. S. Novoselov, S. Roth, and A. K. Geim, Phys. Rev. Lett. **97**, 187401 (2006).

[10] P. Venezuela, M. Lazzeri, and F. Mauri, Phys. Rev. B **84**, 035433 (2011).

[11] H. Zeng, J. Dai, W. Yao, D. Xiao, and X. Cui, Nat. Nanotechnol. **7**, 490 (2012).

[12] K. F. Mak, K. He, J. Shan, and T. F. Heinz, Nat. Nanotechnol. **7**, 494 (2012).

[13] C. V. Raman and K. S. Krishnan, Nature (London) **121**, 501 (1928).

[14] S. A. Asher, M. Ludwig, and C. R. Johnson, J. Am. Chem. Soc. **108**, 3186 (1986).

[15] J. A. Shelnutt, J. Chem. Phys. **72**, 3948 (1980).

[16] J. B. Page, in *Light Scattering in Solids VI*, edited by M. Cardona and G. Güntherodt, Topics in Applied Physics Vol. 68 (Springer, Berlin, 1991), pp. 17–72.

[17] R. M. Martin and L. M. Falicov, in *Light Scattering in Solids I: Introductory Concepts*, edited by M. Cardona, Topics in Applied Physics Vol. 8 (Springer, Berlin, 1983), pp. 79–145.

[18] B. R. Carvalho, L. M. Malard, J. M. Alves, C. Fantini, and M. A. Pimenta, Phys. Rev. Lett. **116**, 089904(E) (2016).

[19] Y. Gillet, M. Giantomassi, and X. Gonze, Phys. Rev. B **88**, 094305 (2013).

[20] E. del Corro, A. Botello-Méndez, Y. Gillet, A. L. Elias, H. Terrones, S. Feng, C. Fantini, D. Rhodes, N. Pradhan, L. Balicas, X. Gonze, J.-C. Charlier, M. Terrones, and M. A. Pimenta, Nano Lett. **16**, 2363 (2016).

[21] H. P. C. Miranda, S. Reichardt, G. Froehlicher, A. Molina-Sánchez, S. Berciaud, and L. Wirtz, Nano Lett. **17**, 2381 (2017).

[22] M. Profeta and F. Mauri, Phys. Rev. B **63**, 245415 (2001).

[23] C. Rice, R. J. Young, R. Zan, U. Bangert, D. Wolverson, T. Georgiou, R. Jalil, and K. S. Novoselov, Phys. Rev. B **87**, 081307 (2013).

[24] L. Liang and V. Meunier, Nanoscale **6**, 5394 (2014).

[25] A. Molina-Sánchez and L. Wirtz, Phys. Rev. B **84**, 155413 (2011).

[26] P. Y. Yu and M. Cardona, *Fundamentals of Semiconductors*, Graduate Texts in Physics (Springer, Berlin, 1999).

[27] M. Lazzeri and F. Mauri, Phys. Rev. Lett. **90**, 036401 (2003).

[28] L. Wirtz, M. Lazzeri, F. Mauri, and A. Rubio, Phys. Rev. B **71**, 241402(R) (2005).

[29] M. Veithen, X. Gonze, and P. Ghosez, Phys. Rev. B **71**, 125107 (2005).

[30] P. Umari, A. Pasquarello, and A. Dal Corso, Phys. Rev. B **63**, 094305 (2001).

[31] S. Baroni, S. De Gironcoli, A. Dal Corso, and P. Giannozzi, Rev. Mod. Phys. **73**, 515 (2001).

[32] Expanding to order n will give scattering rates for n-phonon Raman processes [60].

[33] See Supplemental Material at http://link.aps.org/supplemental/10.1103/PhysRevB.98.161405 for additional details on phonon calculations, the convergence of excitation energies, remnant resonances at the A/B exciton energies, and proof for Eq. (3) in the main text.

[34] $H^{DFT} = (\epsilon_c - \epsilon_v)\delta_{cc'}\delta_{vv'}$, where $\epsilon_{c,v}$ are conduction and valence band energies, respectively.

[35] $H^{BSE} = (\epsilon_{c,GW} - \epsilon_{v,GW})\delta_{cc'}\delta_{vv'} + K_{cv,c'v'}$, where ϵ_{GW} are quasiparticle energies and $K_{cc',vv'}$ is the BSE kernel [51].

[36] A. Compaan and H. J. Trodahl, Phys. Rev. B **29**, 793 (1984).

[37] Y. Gillet, *Ab initio* study of Raman and optical spectra of crystalline materials and their temperature dependence, Ph.D. thesis, Université Catholique de Louvain, 2017.

[38] A. A. Puretzky, L. Liang, X. Li, K. Xiao, K. Wang, M. Mahjouri-Samani, L. Basile, J. C. Idrobo, B. G. Sumpter, V. Meunier, and D. B. Geohegan, ACS Nano **9**, 6333 (2015).

[39] C. Ambrosch-Draxl, H. Auer, R. Kouba, E. Y. Sherman, P. Knoll, and M. Mayer, Phys. Rev. B **65**, 064501 (2002).

[40] A. C. Albrecht, J. Chem. Phys. **34**, 1476 (1961).

[41] R. Bozio, A. Feis, I. Zanon, and C. Pecile, J. Chem. Phys. **91**, 13 (1989).

[42] M. Walter and M. Moseler, arXiv:1806.03840.

[43] *Light Scattering in Solids II*, edited by M. Cardona and G. Güntherodt, Topics in Applied Physics Vol. 50 (Springer, Berlin, 1982).

[44] J. Kürti and H. Kuzmany, Phys. Rev. B **44**, 597 (1991).

[45] S. Gupta, S. N. Shirodkar, D. Kaplan, V. Swaminathan, and B. I. Yakobson, J. Phys.: Condens. Matter **30**, 095501 (2018).

[46] D. A. Strubbe, Optical and transport properties of organic molecules: Methods and applications, Ph.D. thesis, University of California Berkeley, 2012.

[47] S. Ismail-Beigi and S. G. Louie, Phys. Rev. Lett. **90**, 076401 (2003).

[48] J. B. Renucci, R. N. Tyte, and M. Cardona, Phys. Rev. B **11**, 3885 (1975).

[49] D. Xiao, G. B. Liu, W. Feng, X. Xu, and W. Yao, Phys. Rev. Lett. **108**, 196802 (2012).

[50] J. Deslippe, G. Samsonidze, D. A. Strubbe, M. Jain, M. L. Cohen, and S. G. Louie, Comput. Phys. Commun. **183**, 1269 (2012).

[51] M. Rohlfing and S. G. Louie, Phys. Rev. B **62**, 4927 (2000).

[52] P. Giannozzi, S. Baroni, N. Bonini, M. Calandra, R. Car, C. Cavazzoni, D. Ceresoli, G. L. Chiarotti, M. Cococcioni, I. Dabo, A. D. Corso, S. Fabris, G. Fratesi, S. de Gironcoli, R. Gebauer, U. Gerstmann, C. Gougoussis, A. Kokalj, M. Lazzeri, L. Martin-Samos *et al.*, J. Phys.: Condens. Matter **21**, 395502 (2009).

[53] S. Ismail-Beigi, Phys. Rev. B **73**, 233103 (2006).

[54] J. Deslippe, G. Samsonidze, M. Jain, M. L. Cohen, and S. G. Louie, Phys. Rev. B **87**, 165124 (2013).

[55] M. S. Hybertsen and S. G. Louie, Phys. Rev. B **34**, 5390 (1986).

[56] X. Li, J. T. Mullen, Z. Jin, K. M. Borysenko, M. Buongiorno Nardelli, and K. W. Kim, Phys. Rev. B **87**, 115418 (2013).

[57] J. R. Chelikowsky and M. L. Cohen, Phys. Rev. B **10**, 5095 (1974).

[58] G. Antonius and S. G. Louie, arXiv:1705.04245.

[59] A. McCreary, J. R. Simpson, Y. Wang, D. Rhodes, K. Fujisawa, L. Balicas, M. Dubey, V. H. Crespi, M. Terrones, and A. R. Hight Walker, Nano Lett. **17**, 5897 (2017).

[60] Y. Gillet, S. Kontur, M. Giantomassi, C. Draxl, and X. Gonze, Sci. Rep. **7**, 7344 (2017).

[61] P. Cudazzo, L. Sponza, C. Giorgetti, L. Reining, F. Sottile, and M. Gatti, Phys. Rev. Lett. **116**, 066803 (2016).

[62] D. Y. Qiu, T. Cao, and S. G. Louie, Phys. Rev. Lett. **115**, 176801 (2015).

[63] F. Wu, F. Qu, and A. H. MacDonald, Phys. Rev. B **91**, 075310 (2015).